Role of conserved tyrosine lid residues in the activation of the M2 muscarinic acetylcholine receptor

Pham, V.; Habben Jansen, M.C.C.; Thompson, G.; Heitman, L.H.; Christopoulos, A.; Thal, D.M.; Valant, C.

1521-0111/104/3/92–104$35.00
MOLECULAR PHARMACOLOGY

dx.doi.org/10.1124/molpharm.122.000661
Mol Pharmacol 104:92–104, September 2023

Role of Conserved Tyrosine Lid Residues in the Activation of the M_2 Muscarinic Acetylcholine Receptor[S]

Vi Pham, Maria Clazina Cornelia Habben Jansen, Geoff Thompson, Laura H. Heitman, Arthur Christopoulos, David M. Thal, and Celine Valant

Drug Discovery Biology (V.P., G.T., A.C., D.M.T., C.V.), ARC Industrial Transformation Training Centre for Cryo-Electron Microscopy of Membrane Proteins (A.C., D.M.T.), Monash Institute of Pharmaceutical Sciences, Monash University, Parkville, Victoria, Australia; Drug Discovery and Safety, Universiteit Leiden, Leiden, The Netherlands (M.C.C.H.J., L.H.H.); and Neuromedicines Discovery Center, Monash University, Parkville, Victoria, Australia (A.C.)

Received December 7, 2022; accepted June 6, 2023

ABSTRACT

The development of subtype selective small molecule drugs for the muscarinic acetylcholine receptor (mAChR) family has been challenging. The design of more selective ligands can be improved by understanding the structure and function of key amino acid residues that line ligand binding sites. Here we study the role of three conserved key tyrosine residues [$Y104^{3.33}$, $Y403^{6.51}$, and $Y426^{7.39}$ (Ballesteros and Weinstein numbers in superscript)] at the human M_2 mAChR, located at the interface between the orthosteric and allosteric binding sites of the receptor. We specifically focused on the role of the three tyrosine hydroxyl groups in the transition between the inactive and active conformations of the receptor by making phenylalanine point mutants. Single-point mutation at either of the three positions was sufficient to reduce the affinity of agonists by ~100-fold for the M_2 mAChR, whereas the affinity of antagonists remained largely unaffected. In contrast, neither of the mutations affected the efficacy of orthosteric agonists. When mutations were combined into double and triple M_2 mAChR mutants, the affinity of antagonists was reduced by more than 100-fold compared with the wild-type M_2 receptor. In contrast, the affinity of allosteric modulators, either negative or positive, was retained at all single and multiple mutations, but the degree of allosteric effect exerted on the endogenous ligand acetylcholine was affected at all mutants containing $Y426^{7.39}F$. These findings will provide insights to consider when designing future mAChR ligands.

SIGNIFICANCE STATEMENT

Structural studies demonstrated that three tyrosine residues between the orthosteric and allosteric sites of the M_2 muscarinic acetylcholine receptor (mAChR) had different hydrogen bonding networks in the inactive and active conformations. The role of hydroxyl groups of the tyrosine residues on orthosteric and allosteric ligand pharmacology was unknown. We found that hydroxyl groups of the tyrosine residues differentially affected the molecular pharmacology of orthosteric and allosteric ligands. These results provide insights to consider when designing future mAChR ligands.

Introduction

Muscarinic acetylcholine receptors (mAChRs) are class A G protein–coupled receptors (GPCRs) with five subtypes, M_1–M_5, activated by the endogenous neurotransmitter acetylcholine (ACh) (Fredriksson et al., 2003). The M_1, M_3 and M_5 mAChRs preferentially couple to $G\alpha_{q/11}$ proteins, whereas M_2 and M_4 mAChRs preferentially couple to $G\alpha_{i/o}$ proteins (Hulme et al., 1990). Due to their unique distribution throughout the peripheral and central nervous system, mAChRs have been identified as therapeutic targets for several pathophysiological conditions, including schizophrenia, Alzheimer's disease, etc. (Wess et al., 2007; Eglen, 2012). However, a key bottleneck for therapeutic development has been the difficulty in designing small-molecule drugs that specifically target one mAChR subtype over others due to the fact that the orthosteric (endogenous) ligand-binding site is structurally similar across all five receptors (Thal et al., 2016; Vuckovic et al., 2019).

Previous mutagenesis and structural studies of mAChRs have identified key residues that contribute to the binding

This work was funded by the Australian Research Council Discovery Project [Grant DP190102950] (to C.V.), the National Health and Medical Research Council of Australia (NHMRC) Program [Grant APP1150083] (to A.C.), and the Wellcome Trust [Grant 201529/Z/16/Z] (to A.C.). D.M.T. is an Australian Research Council DECRA Fellow [Grant DE170100152] and an NHMRC Early Career Investigator [Grant APP1196951].
No author has an actual or perceived conflict of interest with the contents of this article.
dx.doi.org/10.1124/molpharm.122.000661.
[S] This article has supplemental material available at www.molpharm.aspetjournals.org.

ABBREVIATIONS: ACh, acetylcholine; C_7/3-phth, heptane-1,7-bis(dimethyl-3′-phthalimidopropylammonium); DMEM, Dulbecco's modified Eagle's medium; GTPγS, guanosine 5′-3-O-(thio)triphosphate; LY-2119620, 3-amino-5-chloro-N-cyclopropyl-4-methyl-6-[2-(4-methyl-1-piperazinyl)-2-oxoethoxy]-thieno[2,3-b]pyridine-2-carboxamide; mAChR, muscarinic acetylcholine receptor; NAM, negative allosteric modulator; NMS, N-methylscopolamine; PAM, positive allosteric modulator; pERK1/2, phosphorylated extracellular signal-regulated kinase ½; WT, wild type.

and signaling of orthosteric and allosteric ligands (Haga et al., 2012; Kruse et al., 2012, 2013; Hulme, 2013; Thal et al., 2016; Suno et al., 2018; Maeda et al., 2019; Vuckovic et al., 2019). The tyrosine lid ($Y^{3.33}$, $Y^{6.51}$, $Y^{7.39}$; superscripts refer to Ballesteros-Weinstein residue numbering system (Ballesteros and Weinstein, 1995) is a conserved mAChR motif that contributes to the "roof" of the orthosteric site and the "floor" of the extracellular allosteric site (Burger et al., 2018). The size of the mAChR orthosteric site is typically larger when bound to antagonists and smaller when bound to agonists, which manifests as a different arrangement of the tyrosine lid residues in the inactive and active conformations of the receptor (Kruse et al., 2013). In the inactive conformation, the tyrosine residues are too far apart to directly interact and instead likely indirectly interact together through interactions with shared water molecules, as observed in the high-resolution structure of the M_2 mAChR bound to the antagonist N-methylscopolamine (NMS) (Suno et al., 2018) (Fig. 1). The result is a more open conformation of the tyrosine lid that permits direct access of water molecules to the orthosteric site. In contrast, in the active iperoxo-bound conformation of the M_2 mAChR, the tyrosine lid residues move inward, forming hydrogen bond interactions with each other (Fig. 1). Prior mutagenesis studies have explored the role of the tyrosine lid residues in orthosteric and allosteric ligand pharmacology at several mAChRs by making single alanine point mutations (Matsui et al., 1995; Bourdon et al., 1997; Avlani et al., 2010; Gregory et al., 2010; Nawaratne et al., 2010; Tautermann et al., 2013; Abdul-Ridha et al., 2014; Keov et al., 2014; Thal et al., 2016). These tyrosine-to-alanine mutations were disruptive and affected the pharmacology of both orthosteric and allosteric ligands.

Despite the structural and pharmacological importance of the tyrosine lid for all mAChR subtypes, there has been no systematic investigation into the role the hydroxyl groups of the tyrosine lid play in the binding and signaling of different orthosteric and allosteric ligands. A prior study at the M_2 mAChR (Vogel et al., 1997) suggested that the $Y403^{6.51}F$ mutant was able to reduce the affinity of orthosteric agonists but not their ability to signal. This finding was in contrast to an earlier study at the M_3 mAChR (Wess et al., 1992), which showed that $Y533^{6.51}F$ mutant promoted only a 10-fold reduction in orthosteric agonists' binding (pK_I) but >100-fold reduction in their signaling properties. Therefore, we aimed to validate the pharmacological importance of the hydroxyl groups of the tyrosine lid residues at the M_2 mAChR by mutating the tyrosine residues to phenylalanine and generating seven mutated receptor constructs that include three single mutants ($Y104^{3.33}F$, $Y403^{6.51}F$, $Y426^{7.39}F$), three double mutants (Y104F+Y403F, Y104F+Y426F, Y403F+Y426F), and one triple mutant (Y104F+Y403F+Y426F). The pharmacology of the M_2 mAChR was investigated using [^{3}H]-NMS equilibrium binding and three different signaling assays: phosphorylated extracellular signal-regulated kinase 1/2 (pERK1/2), [^{35}S]-guanosine 5′-O-[γ-thio]triphosphate ([^{35}S]GTPγS) binding, and β-arrestin 2 recruitment. The impact of the mutations on agonist and antagonist binding and signaling properties were assessed, as well as the allosteric properties between allosteric modulators and ACh. Our results reveal that removing the hydroxyl group from any of the three tyrosine residues resulted in a dramatic reduction of the affinity of orthosteric agonists ACh and iperoxo but only subtle changes for the antagonists atropine and NMS. In contrast, the ground-state binding affinity of allosteric modulators for the prototypical negative allosteric modulator (NAM) C_7/3-phth [heptane-1,7-bis(dimethyl-3′-phthalimidopropylammonium)] and the positive allosteric modulator (PAM) LY-2119620 (3-amino-5-chloro-N-cyclopropyl-4-methyl-6-[2-(4-methyl-1-piperazinyl)-2-oxoethoxy]-thieno[2,3-b]pyridine-2-carboxamide) were unaffected; however, the PAM effect between LY-2119620 and ACh was differentially altered for $Y104^{3.33}F$ and $Y426^{7.39}F$. The mechanism of receptor coupling to intracellular transducers remained unaffected by any of the mutations.

Materials and Methods

Materials. Chinese hamster ovary Flp-In cells were purchased from Invitrogen (Carlsbad, CA). Dulbecco's modified Eagle's medium (DMEM) and fetal bovine serum (FBS) were purchased from ThermoTrace (Melbourne, Australia). Hygromycin-B was purchased from Roche Applied Science (Mannheim, Germany). Phosphate-buffered-saline (PBS) and Versene (PBS supplemented with 0.2% EDTA) were made in house (Melbourne, Australia). Primers used for generating mutant receptors were purchased from GeneWorks (Australia). The AlphaScreen Surefire phosphor-ERK1/2 reagents were kindly provided by TGR Biosciences (Adelaide, Australia). AlphaScreen streptavidin donor beads and anti-IgG (protein A) acceptor beads, [^{3}H]N-methylscopolamine ([^{3}H]NMS; specific activity 80 Ci/mmol) and [^{35}S]-guanosine 5′-O-[γ-thio]-triphosphate) ([^{35}S]GTPγS; 1000 Ci/mmol) were purchased from PerkinElmer Life and Analytical Sciences (Waltham, MA). Acetylcholine and atropine were purchased from Sigma-Aldrich (St. Louis, MO). LY-2119620 was a generous gift and was synthesized at Eli Lilly & Co. (Indianapolis, IN). C_7/3-phth was synthesized at the Monash Institute of Pharmaceutical Sciences (Melbourne, Australia) as a generous gift from Frederick Mitchelson. All other chemicals were from Sigma-Aldrich (St. Louis, MO).

Receptor Mutagenesis, Stable Cell Line Generation, and Cell Culture. Mutant receptors were generated as previously described (Valant et al., 2012) using QuikChange site-directed mutagenesis (Invitrogen), and all sequences were confirmed by DNA sequencing (Australian Genome Research Facility). All receptor constructs, wild type (WT) and mutant, were stably expressed in CHO Flp-In cells using Flp-In Gateway technology system and selected using 600 μg/ml of hygromycin B. Cells were maintained in DMEM supplemented with 5% FBS and 600 μg/ml hygromycin B at 37°C in a humidified incubator (5% CO_2, 95% O_2). Cells were regularly monitored for mycoplasma contamination using the Lonza MycoAlert Mycoplasma Detection Kit (Lonza, Basel, Switzerland).

Whole-Cell Radioligand Binding Assay. Saturation binding assays were first performed to estimate receptor expression and affinity of radiolabeled [^{3}H]-N-methyl scopolamine (NMS). Cells were seeded at 20,000 cells per well in a 96-well Isoplate (PerkinElmer), and allowed to adhere overnight. Plates were washed once with phosphate-buffered saline (PBS) and incubated overnight at room temperature with 0.03–10 nM [^{3}H]-NMS (PerkinElmer, specific activity 80 Ci/mmol) in 100 μl of binding buffer (137 mM NaCl, 2.7 mM KCl, 1 mM $MgCl_2$, 12 mM $NaHCO_3$, 1.8 mM $CaCl_2$, 5.5 mM D-glucose, 0.2 mM Na_2HPO_4, 1.85 mM $CaCl_2$, 10 mM HEPES, adjusted to pH 7.4 with 10 mM NaOH). Equilibrium inhibition binding assays were carried out to determine the affinity of unlabeled ligands. Cells were incubated with increasing concentrations of each ligand in the presence of [^{3}H]-NMS at approximately K_D concentrations as determined for each receptor in saturation binding experiments; 0.24 nM for WT, 1.20 nM for $Y104^{3.33}F$, 0.48 nM for $Y403^{6.51}F$, and 3.16 nM for $Y426^{7.39}F$) in a final volume of 100 μl. Nonspecific binding was determined by the addition of 10 μM atropine. After washing in cold 0.9% NaCl, cells were solubilized in 100 μl per well of Ultima Gold (PerkinElmer), and radioactivity (cpm) was measured in a MicroBeta2 counter (PerkinElmer). The individual data were normalized to the

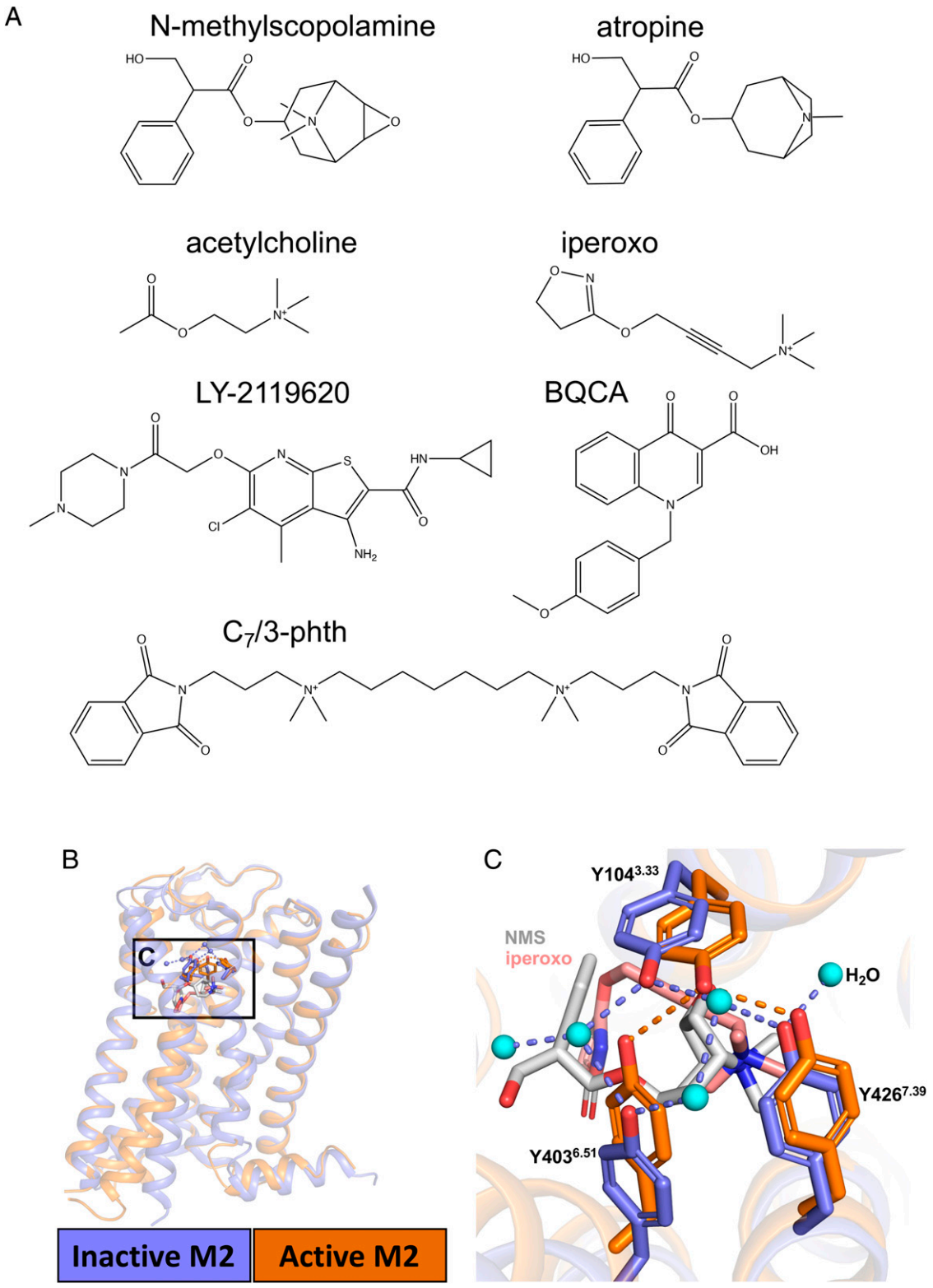

Fig. 1. Ligands and residues investigated in this study. (A) Structures of all ligands investigated in the current study: two antagonists [N-methylscopolamine (NMS) and atropine], two agonists [the endogenous neurotransmitter acetylcholine (ACh) and the high affinity synthetic agonist iperoxo], and two allosteric modulators [the M_2/M_4 mAChR positive allosteric modulator (PAM) of ACh response (LY-2119620) and C_7/3-phth, a nonselective negative allosteric modulator (NAM) of ACh response]. (B, C) Comparison of the tyrosine lid residues from the inactive state structure of the M_2 mAChR bound to NMS (residues and hydrogen bonds colored blue, water molecules cyan, and NMS white; PDB: 5ZK8) and the tyrosine lid residues from the active state of the M_2 mAChR bound to the high-affinity agonist iperoxo (residues and hydrogen bonds colored orange and iperoxo peach; PDB: 4MQS). Residues $Y104^{3.33}$, $Y403^{6.51}$, and $Y426^{7.39}$ differentially engage with agonists and antagonists at the M_2 mAChR.

total binding in cpm in the presence of [^{3}H]-NMS without any ligand (100%) and to the nonspecific remaining binding in cpm in the presence of [^{3}H]-NMS and 10 μM atropine (0%).

(pERK1/2) Assays. The AlphaScreen SureFire Kit was used to quantify phosphorylated ERK1/2 (pERK1/2). Cells expressing the M_2 WT or mutants were seeded at 20,000 cells per well into transparent 96-well plates and grown overnight at 37°C, 5% CO_2. Cells were washed once with PBS and incubated in serum-free DMEM at 37°C for 4 hours to allow FBS-stimulated pERK1/2 levels to subside. Initial ERK1/2 phosphorylation time course experiments were performed to determine the time of the peak pERK1/2 response for each ligand and each cell line (5 minutes for all ligands and cell lines tested; data not shown). For concentration-response curves or functional interaction experiments, cells were stimulated for 5 minutes with increasing concentrations of ACh in the absence or presence of increasing concentrations of interacting ligands (atropine, NMS, C7/3-phth, or LY-2119620) on the heating platform at 37°C for 5 minutes, the time at which the peak response was induced. When the interacting ligand did not produce a peak in time-course experiments, ligands were incubated for 15 minutes prior to agonist stimulation. For all experiments, 10% (v/v) FBS was used as the positive control and vehicles controls were also performed. The reaction was terminated by removal of media/ligands and lysis of cells with 50 μl of the SureFire lysis buffer (TGR Biosciences), and 5 μl of this lysate was transferred to a 384-well white ProxiPlate (PerkinElmer). In reduced lighting condition, a mixture of SureFire activation buffer, Surefire reaction buffer, and acceptor and donor beads were prepared in a ratio of 100:600:3:3 (v/v/v) and added to the lysate for a lysate/mixture ratio of 5:8 (v/v). Plates were incubated for 1–1.5 hours at 37°C before the fluorescence signal (cps) was measured on the Envision plate reader (PerkinElmer) using standard AlphaScreen settings. Raw data were collected as counts per second (cps). The detection window for pERK1/2 was approximately 10-fold between basal (~12000 cps) and maximal ACh-induced response (~120,000 cps). Individual data were normalized to the maximal response elicited by ACh.

Cell Membrane Preparation and [^{35}S]GTPγS Binding Assays. Cell membranes of the M_2 mAChR WT and mutants were prepared for [^{35}S]GTPγS assay. Briefly, cells were grown to confluence and washed with warm PBS (pH7.4). Cells were detached with warm Versene and pelleted by centrifugation at 350 *g* for 3 minutes at room temperature. The pellet was resuspended in ice-cold homogenization buffer (20mM HEPES, 10mM $MgCl_2$, 100mM NaCl, 1mM EGTA, adjusted to pH 7.4 with 10 mM NaOH) and homogenized for three 10-second intervals at maximum setting, with a 30-second cooling period on ice between each burst. The homogenates were centrifuged at 600 *g* for 10 minutes at 4°C, the pellet was discarded, and the supernatant was recentrifuged at 20,000 *g* at 4°C for 1 hour. The final pellet was resuspended in 20 mM HEPES, 10 mM $MgCl_2$, and 100 mM NaCl, adjusted to pH 7.4 with 10 mM NaOH using a syringe. Protein concentration was determined using bicinchoninic acid quantification method with bovine serum albumin (BSA) as the standard. Aliquots were stored at −80°C until required for [^{35}S]GTPγS assay.

[^{35}S]GTPγS binding experiments were performed using cell-membrane homogenates (25 μg) equilibrated in 200 μl [^{35}S]GTPγS assay buffer (20 mM HEPES, 10 mM $MgCl_2$ and 100 mM NaCl, 30 μg/ml Saponin, and 0.1% BSA, adjusted to pH7.4 with 10 mM NaOH) containing varying concentrations of the orthosteric ligand ACh alone or in presence of the allosteric modulator LY-2119620 and 30 μM guanosine 5′-diphosphate sodium salt (GDP) at room temperature for 30 minutes. After 30 minutes, 50 μl of [^{35}S]GTPγS (0.3 nM) was added and incubation was continued for another 60 minutes at room temperature. Incubation was terminated by rapid filtration with a Packard plate harvester onto 96-well GF/C filter plates followed by three washes with ice-cold Tris buffer (50 mM Tris-HCl, 10mM $MgCl_2$, 100 mM NaCl, pH7.6). After drying for 3 hours at 55°C, the GF/C filter plates were sealed with melt-on scintillator sheets. Bound [^{35}S] was solubilized in 40 μl Microscint-20, and radioactivity (in cpm) was measured in a MicroBeta2 counter (PerkinElmer Life Sciences). The response window for GTPγS detected was approximately 3-fold between the basal level (vehicle only, ~7100 cpm) to the maximal response (E_{max} of ACh, ~23,000 cpm). Individual data were normalized to the maximal response elicited by ACh.

***β*-Arrestin 2 Recruitment Assays.** Parental Flp-In CHO cells seeded in 10-cm dishes were transiently transfected with DNA constructs [NanoLuc-tagged hM_2 mAChR: yellow fluorescent protein (YFP)-tagged β-arrestin-2 (4:1 μg)]. At 24 hours after transfection, cells were plated on the white culture plates-96 (PerkinElmer, Waltham, MA) to start the assay the following day after washing and stimulating the cells with prewarmed Hanks' balanced salt solution (HBSS) buffer (HBSS 1×; 37°C). The plates were incubated with NanoBRET Nano-Glo Substrate (Promega, Madison, WI), and the bioluminescence resonance energy transfer (BRET) signals were measured on a LUMIstar OMEGA microplate reader (BMG LABTECH, Mornington, Victoria, Australia) for approximately 20 minutes. The fluorescence was measured at an excitation wavelength of 475 nm and emission wavelength of 535 nm. The BRET ratio was calculated as the emission values (in relative light units, RLU) divided by the excitation values (RLU). The background values were negligible. The detection window for β-arrestin 2 was approximately ~0.04 with the basal level (vehicle only) of ~0.51 and maximal response (E_{max} of ACh) of ~0.56. Individual data were normalized to the maximal response elicited by ACh.

Data Analysis. Experiments in the current study were conducted in an exploratory manner and were not designed to test a prespecified statistical null hypothesis. As such, reported *P* values in this study should be considered as descriptive. Group sizes (*n*) reflect the individual number of independent experiments performed in duplicate, which was decided prior to project commencement based on previous experience. Differences in group sizes between treatments or mutants are due to a number of factors, including the use of different cell batches and subsequent confirmation of multiple cell batches for their reproducibility as well as the need to include a reference ligand for each set of experiments. Only group sizes equal to or greater than 3 were used for statistical analysis.

All graphs were analyzed using nonlinear regression lines in GraphPad Prism 9.02 (GraphPad Software Inc., San Diego, CA). A one-site saturation binding model was globally fitted to the total and nonspecific [^{3}H]-NMS binding data to derive estimates of the radioligand equilibrium dissociation constant (pK_D) and the maximal density of binding sites (B_{max}) for the human M_2 mAChR WT and the mutant receptors. The one-site inhibition mass action curve to determine inhibitor potency (pIC_{50}) estimates was fitted to the radioligand inhibition binding data, which were then converted to pK_I values as appropriate (Cheng and Prusoff, 1973). A simple allosteric ternary complex model was fitted to the radioligand binding curves with C_7/3-phth to derive estimates of allosteric modulator affinity (pK_B) and cooperativity ($Log\alpha_{NMS}$) between the compound and radioligand, where $\alpha_{NMS} > 1$ denotes positive cooperativity, $0 > \alpha_{NMS} > 1$ denotes negative cooperativity, and $\alpha_{NMS} = 1$ denotes neutral cooperativity (Christopoulos and Kenakin, 2002). A three-parameter logistic equation was fitted to the concentration-response curves to derive ligand potency (pEC_{50}) estimates. Subsequently, to compare agonist profiles between the wild-type and mutant receptors in terms of separating effects on affinity from signaling efficacy, an operational model of agonism was fitted to agonist concentration-response curves to estimate efficacy in the system ($Log\tau$) (Black and Leff, 1983). The Waud/Schild equation (Waud and Parker, 1971) was fitted to the functional interactions between ACh and orthosteric antagonists to derive functional affinity (pA_2) and Schild slope of interaction (s_s). The operational model of allosterism (Leach et al., 2007) was fitted to the functional interactions between ACh and allosteric modulators. All affinities, potencies, and cooperativity parameters were estimated as logarithms. Repeated measures one-way ANOVA with Dunnett's

multiple comparisons tests were performed to determine significant differences ($P < 0.05$) and mentioned in the footnotes of each table. All post-test comparisons were chosen before any data were observed. All values reported in the tables are mean ± S.D. for the indicated number (n) of independent experiments performed in duplicate.

Results

The Hydroxyl Groups of Tyrosine Lid Residues Differentially Affect the Binding Affinity of mAChR Ligands. All mutant M_2 mAChR cell lines were characterized in saturation binding experiments with [^{3}H]-N-methylscopolamine ([^{3}H]-NMS) to determine the binding affinity (pK_D) of the radiolabeled antagonist and expression (B_{max}) of the WT and mutant M_2 mAChRs (Supplemental Fig. 1). The WT and single-mutant receptors (Y104$^{3.33}$F, Y403$^{6.51}$F, and Y426$^{7.39}$F) showed similar cell surface expression levels, suggesting that single mutations had no effect on receptor expression (Supplemental Table 1). The binding affinity of [^{3}H]-NMS was modestly affected at two of the three single mutant receptors, Y104$^{3.33}$F and Y426$^{7.39}$F, with a 5- to 10-fold loss in [^{3}H]-NMS binding affinity compared with WT, respectively. Importantly, the multiple mutant receptor constructs that combined either two or three of the tyrosine mutations did not allow for separation between total and nonspecific [^{3}H]-NMS binding, thus not allowing for determination of either the binding affinity of [^{3}H]-NMS or receptor expression. The M_2 mAChR constructs did not contain any antibody epitope tags preventing further investigation into receptor expression. The impaired binding of [^{3}H]-NMS at the double and triple mutants was similar to single-point alanine mutations of tyrosine lid residues at the M_3 mAChR for which the affinity of NMS was reduced by several orders of magnitude (Tautermann et al., 2013).

We next performed equilibrium competition binding assays on the single mutants using several orthosteric ligands: two antagonists (NMS and atropine) and two agonists (ACh and the high-affinity agonist iperoxo) (Fig. 2). All orthosteric ligands fully inhibited [^{3}H]-NMS binding at the WT and single-mutant receptors (Fig. 2, A–D). However, the binding affinity (pK_I) of the orthosteric ligands differed compared with the WT receptor depending on whether the ligand was an agonist or an antagonist (Fig. 2E; Table 1). NMS and atropine were modestly affected by the Y104$^{3.33}$F mutation (5- to 10-fold), whereas Y426$^{7.39}$F mostly affected NMS binding (10-fold). In contrast, all three mutations (Y104$^{3.33}$F, Y403$^{6.51}$F, and Y426$^{7.39}$F) reduced the binding affinity of the agonists ACh and iperoxo by more than 100-fold.

Hydroxyl Groups from the Tyrosine Lid Residues Do Not Drive the Coupling of the M_2 mAChR with Intracellular Transducers. We next investigated the role of the hydroxyl group of each tyrosine residue on the ability of the M_2 mAChR to activate intracellular transducers. We performed concentration-response curves with ACh in three functional assays. Proximal receptor activation was measured by [^{35}S]GTPγS binding and β-arrestin 2 recruitment assays, and phosphorylation of the extracellular signal-regulated kinase (ERK)1/2 assay was used to measure a highly amplified signaling pathway distal to receptor activation (Fig. 3). At the WT receptor, the rank order in the potency estimates of ACh between the three assays (Fig. 3A) was pERK1/2 > [^{35}S]GTPγS > β-arrestin 2 recruitment (Supplemental Table 2). In line with our radioligand binding findings, the three mutant receptors (Y104$^{3.33}$F, Y403$^{6.51}$F, and Y426$^{7.39}$F) reduced the potency of ACh by more than 100-fold in all three signaling assays compared with the WT receptor (Fig. 3, B–D; Supplemental Table 2). To further explore the impact the hydroxyl groups had on the M_2 mAChR signaling, we quantified the efficacy (τ) of ACh for the two pathways for which the endogenous ligand was a full agonist by applying an operational model of agonism to the pERK1/2 and [^{35}S]GTPγS binding data (Fig. 3F; Supplemental Table 2). No significant difference in ACh efficacy was observed in pERK1/2 and [^{35}S]GTPγS binding assays at either of the single M_2 mAChR mutants, suggesting that tyrosine lid mutations only affected the affinity of ACh and not its ability to activate the human M_2 mAChR.

The Loss of Multiple Hydroxyl Groups within the Tyrosine Lid Further Reduce Agonist Potency and Antagonist Functional Affinity. Since none of the multiple mutant constructs were able to be characterized in radioligand binding assays, we used the highly amplified pERK1/2 assay for further characterization of these mutants (Fig. 4A). All four mutant receptors produced a functional response that could be detected in this assay, albeit with reduced agonist potency estimates compared with the WT receptor (Supplemental Table 2). Thus, despite a lack of detectable [^{3}H]-NMS binding, these results indicate the receptor constructs are expressed and functional. We next performed ligand interaction experiments between ACh and the two antagonists, NMS and atropine, to allow for the quantification of functional affinity estimates (pA_2) (Fig. 4, B–F; Supplemental Fig. 2). In all instances, increasing concentrations of atropine induced a parallel rightward shift of the ACh-mediated concentration-response curve with a Schild slope equal to 1 ($s = 1$). Functional affinity estimates were more than 10-fold lower than the WT receptor (Fig. 4G; Table 1). Similar results were observed with NMS (Supplemental Fig. 2). When combining Y104$^{3.33}$F and Y426$^{7.39}$F, as in Y104F+Y426F, and the triple mutant, the degree of reduction of the affinity of NMS was more pronounced.

Tyrosine Lid Residues Play a Minimal Role in the Binding Affinity of the Prototypical NAM C_7/3-phth. We next investigated the role of the tyrosine lid residues with the prototypical NAM C_7/3-phth. In radioligand binding assays, C_7/3-phth appeared to fully inhibit [^{3}H]-NMS at the WT and three single-mutant constructs, suggesting that the modulator exhibits high negative cooperativity with the radioligand and that this property is independent of the hydroxyl group of the tyrosine lid residues. To quantify the binding affinity (pK_B) of C_7/3-phth, we applied an allosteric ternary complex model to fit the data. None of the mutations (Y104$^{3.33}$F, Y403$^{6.51}$F, or Y426$^{7.39}$F) affected the affinity of the NAM (Fig. 5, A and B; Table 1). Similar to atropine and NMS, we also calculated the functional affinity of the NAM at the combined mutants using pERK1/2 assays (Fig. 5, C–G). All functional cooperativity estimates were consistent with extremely high negative cooperativity with ACh ($\alpha\beta \rightarrow 0$), and all but one affinity estimate remained unchanged (Table 1). Statistical analysis of the affinity estimates showed that the affinity of C_7/3-phth was increased by nearly 10-fold at the triple mutant, Y104F+Y403F+Y426F (Fig. 5H).

Tyrosine Lid Residues Differentially Engage with the PAM LY-2119620. To assess the role of the tyrosine lid residues with PAMs such as LY-2119620, we performed functional interactions between ACh and LY-2119620 in pERK1/2 assays

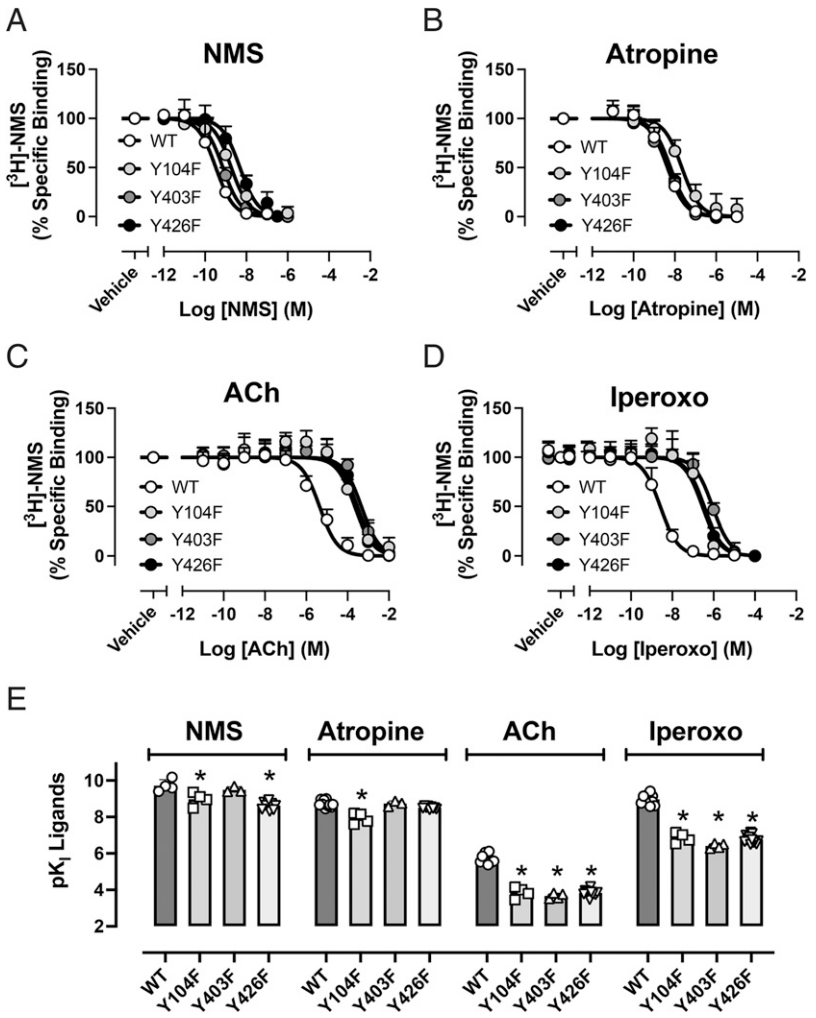

Fig. 2. Binding parameter of mAChR orthosteric ligands are differentially affected by mutations of each of the tyrosine residues into phenylalanine at the M_2 mAChR. Inhibition binding curves at the M_2 mAChR WT and all three single mutants with NMS (A), atropine (B), ACh (C), and iperoxo (D). Data represent the mean ± S.D. of indicated number of experiments performed in duplicate and normalized to vehicle only (100%) and 10 μM atropine (0%). Grouped sizes are denoted in Table 1. Data were empirically fitted to a one-site inhibition mass action curve to determine inhibitor potency (IC_{50}) estimates, which were then converted to K_I values as appropriate using the Cheng/Prusoff correction. (E) Binding affinity of mAChR orthosteric ligands at the M_2 mAChR WT, and three single phenylalanine mutants. *Significantly different compared with WT, $P < 0.05$, one-way ANOVA with Dunnett's post hoc test.

(Fig. 6). As previously observed, increasing concentrations of LY-2119620 induced a significant leftward shift of the ACh-mediated concentration-response curve at the WT receptor (Fig. 6A). Fitting the operational model of allosterism to the data, we confirmed that LY-2119620 binds with micromolar affinity ($pK_B = 5.24 \pm 0.42$) and positive cooperativity with ACh ($Log\alpha\beta = 1.46 \pm 0.51$; Table 2). Interestingly, identical interactions at all seven M_2 mAChR mutants (singles, doubles, and triple), revealed no differences in the affinity of the PAM (Fig. 6, B–I; Table 2). However, the cooperativity between the PAM and ACh was slightly reduced at $Y104^{3.33}F$ yet increased at $Y426^{7.39}F$ and two out of the three other mutants containing $Y426^{7.39}F$ (Y104F+Y426F and Y403F+Y426F) (Fig. 6J; Table 2). Although not significant, the cooperativity with the triple mutant increased as well. Comparing the functional cooperativity of $Y426^{7.39}F$ to the Y104F+Y426F ($P = 1.00$) and Y403F+Y426F ($P = 0.96$) showed no differences, suggesting that the observed increase in cooperativity was predominantly driven by $Y426^{7.39}F$ at the multiple mutant constructs.

Since $Y104^{3.33}F$ and $Y426^{7.39}F$ appeared to alter the degree of cooperativity between LY-2119620 and ACh, we selected these two receptor mutants to assess the effect that the tyrosine lid residues have on the transmission of the PAM effect in the [^{35}S]GTPγS binding and β-arrestin 2 recruitment assays (Supplemental Fig. 3; Table 2). In both assays, we fitted the operational model of allosterism to the data (Supplemental Fig. 3, A–F). All LY-2119620 affinity estimates (pK_B) for $Y104^{3.33}F$ and $Y426^{7.39}F$ in both [^{35}S]GTPγS binding and β-arrestin 2 recruitment were not significantly different from the WT receptor (Supplemental Fig. 3, G and I). Similar to the pERK1/2 data, the functional cooperativity between ACh and LY-2119620 followed identical trends with lower cooperativity for $Y104^{3.33}F$ and higher cooperativity for $Y426^{7.39}F$ (Supplemental Fig. 3, H and J).

Discussion

Here we provide a structure-function study of the M_2 mAChR, specifically focusing on the role of the hydroxyl

TABLE 1

Pharmacological parameters of binding affinity (pK_I) of the orthosteric antagonists NMS and atropine, orthosteric agonists ACh and Iperoxo, and negative allosteric modulator (NAM) C_7/3-phth (pK_B) in radioligand binding assays; and functional affinity of the orthosteric antagonists NMS and atropine (pA_2) and NAM C_7/3-phth (pK_B) in pERK1/2 assays

Values represent the mean ± S.D. of indicated number (n) of independent experiments performed in duplicate.

	pK_I[a]				pK_B[b]
Receptor	NMS	Atropine	Iperoxo	ACh	C_7/3-phth
M_2 WT	9.72 ± 0.33 (n = 4)	8.73 ± 0.18 (n = 11)	8.97 ± 0.26 (n = 12)	5.74 ± 0.25 (n = 11)	6.87 ± 0.24 (n = 7)
$Y104^{3.33}F$	8.97 ± 0.37 (n = 4)*	7.93 ± 0.30 (n = 4)*	6.86 ± 0.28 (n = 4)*	3.86 ± 30 (n = 4)*	7.18 ± 0.18 (n = 4)
$Y403^{6.51}F$	9.49 ± 0.16 (n = 3)	8.73 ± 0.15 (n = 3)	6.41 ± 0.13 (n = 4)*	3.67 ± 0.15 (n = 4)*	7.00 ± 0.22 (n = 3)
$Y426^{7.39}F$	8.62 ± 0.21 (n = 9)*	8.50 ± 0.07 (n = 9)	6.77 ± 0.22 (n = 12)*	3.84 ± 0.22 (n = 12)*	6.74 ± 0.21 (n = 3)
	pA_2[c]				pK_B[b]
Receptor	NMS		Atropine		C_7/3-phth
M_2 WT	9.82 ± 0.22 (n = 4)		8.85 ± 0.18 (n = 4)		6.54 ± 0.54 (n = 13)
Y104F+Y403F	8.26 ± 0.18 (n = 3)*		7.51 ± 0.17 (n = 3)*		6.59 ± 0.20 (n = 5)
Y104F+Y426F	7.41 ± 0.25 (n = 3)*		7.57 ± 0.34 (n = 3)*		6.72 ± 0.31 (n = 5)
Y403F+Y426F	8.03 ± 0.31 (n = 3)*		7.88 ± 0.25 (n = 3)*		6.32 ± 0.28 (n = 4)
Y104F+Y403F+Y426F	7.28 ± 0.39 (n = 3)*		7.11 ± 0.26 (n = 3)*		7.39 ± 0.26 (n = 4)*

[a]Negative logarithm of the orthosteric ligand equilibrium dissociation constant.
[b]Negative logarithm of the allosteric ligand equilibrium dissociation constant.
[c]Negative logarithm of the orthosteric antagonist functional affinity.
*Significantly different compared with WT receptor, $P < 0.05$, one-way ANOVA with Dunnett's post hoc test.

group of the three tyrosine residues located at the interface between the orthosteric and allosteric binding sites. We report that antagonists and agonists of the M_2 mAChR are affected differentially by these key residues. The antagonists NMS and atropine were only marginally affected by the loss of the tyrosine hydroxyl groups in the single mutant receptors (i.e., $Y104^{3.33}F$, $Y403^{6.51}F$, and $Y426^{7.39}F$). To some extent, only subtle changes in antagonist binding affinity were expected, as removal of the hydroxyl group in either of the tyrosine to phenylalanine mutations would only disrupt local interactions with water molecules, as seen in the high-resolution structure of the M_2 mAChR bond to NMS (PDB: 4ZKC) (Suno et al., 2018). However, the loss of multiple hydroxyl groups as seen in the double and triple mutants had dramatic effects on the affinity of antagonists, with reductions in affinity estimates as large as 100-fold compared with the WT receptor. This was observed for both atropine (Fig. 4, B–G) and NMS (Supplemental Fig. 2) and more noticeable at the $Y104^{3.33}F$ and $Y426^{7.39}F$ mutants, which are two key tyrosine residues. This was most likely due to a synergistic effect of the loss of interactions between $Y104^{3.33}$ and $Y426^{7.39}$ and nearby water molecules (Fig. 1), which stabilize the partial closure of the tyrosine lid. These results were not dissimilar from previous work at the M_3 mAChR, in which the tyrosine lid residues were individually mutated to alanine and resulted in large losses in the binding affinity of the antagonist tiotropium and NMS due to the lid becoming more dynamic and facilitating their dissociation (Tautermann et al., 2013). These large reductions in antagonist affinity, particularly for NMS, explain why we were not able to detect specific [^{3}H]-NMS binding at the multiple mutant M_2 mAChR constructs.

In contrast, the agonists iperoxo and ACh were dramatically affected by the loss of the tyrosine lid hydroxyl groups, with a more than 100-fold reduction in their binding affinity (Fig. 2). These findings are in concordance with two previous studies focusing specifically on $Y^{6.51}F$ at the M_3 and M_2 mAChR, which highlighted that this hydroxyl group is important for ACh binding, although more so for the M_2 versus the M_3 mAChR (Wess et al., 1992; Vogel et al., 1997). These results confirm the importance of the conformation of tyrosine lid residues, which move closer together to form hydrogen bond interactions in the ACh- and iperoxo-bound mAChR conformations (Kruse et al., 2012; Maeda et al., 2019). From the structures, it is apparent that the loss of any hydroxyl group would lead to the disruption of the hydrogen bond network as seen in Fig. 1C, resulting in the observed loss of agonist binding affinity.

Further confirmation of the importance of the tyrosine lid residues for the binding of agonists at mAChRs comes from a recent structure-based drug discovery program at the M_1 mAChR. A high-resolution structure of the M_1 mAChR bound to the bulkier agonist 77-LH-28-1 revealed a ligand-pose where the piperidine ring of 77-LH-28-1 breaks through the tyrosine lid of the M_1 mAChR (Brown et al., 2021) into a nearby subpocket. Further SAR and structural work revealed that exploiting the rearranged tyrosine lid and nearby subpocket improved agonist selectivity over the M_2 and M_3 mAChR subtypes.

To examine the role of the tyrosine lid residues on the transmission of agonist activity, we performed three distinct functional assays that have different degrees of amplification (Fig. 3). The rank order of potencies for the three different assays were pERK1/2 > [^{35}S]GTPγS binding > β-arrestin 2 recruitment (Supplemental Table 2). The rank order of potency estimates observed at the M_2 WT were identical within each receptor mutant, suggesting that the hydroxyl groups of the tyrosine lid residues were not directly involved in the global mechanism of activation of the M_2 mAChR and that the reductions in potency observed in functional assays are almost completely due to the lower affinity of ACh for the tyrosine lid M_2 mAChR mutants (Table 1). To validate this observation, we quantified the efficacy parameter of ACh (τ) (Black and Leff, 1983). In contrast to the binding affinity of mAChR ligands, the efficacy of ACh remained unaffected (Fig. 3). Our findings are supported by a previous study (Vogel et al., 1997) suggesting that $Y403^{6.51}F$ had little to no bearing on the coupling ability of the M_2 mAChR with its traditional intracellular partners. Unfortunately, since no binding affinities were quantified for the multiple mutants, we could not

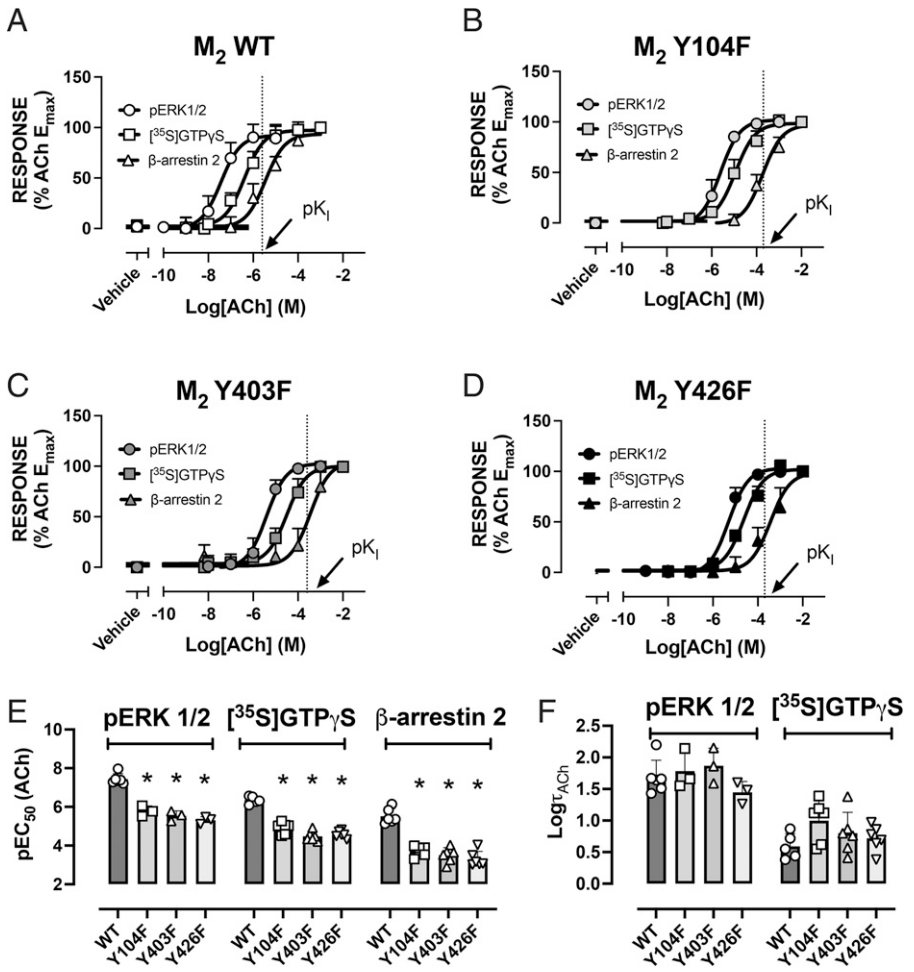

Fig. 3. M_2 mAChR coupling with intracellular effectors. Concentration-response curves of ACh at the M_2 mAChR WT (A), Y104F (B), Y403F (C), and Y426F (D) in three distinct functional pathways: β-arrestin 2 recruitment, [^{35}S]GTPγS binding, and ERK1/2 phosphorylation. Arrow pointing at the x-axis (and vertical dash line) highlight the binding affinity estimate and the ~50% receptor occupancy quantified in radioligand binding assays (Fig. 2C). Data represent mean ± S.D. of indicated number of experiments performed in duplicate and normalized to the maximal response of ACh (100%) and buffer only (0%). Grouped sizes are denoted in Supplemental Table 2. Data were fitted to the three-parameter logistic equation to quantify potency estimates. (E) Potency (pEC_{50}) of ACh in all three signaling assays at each receptor construct. (F) Efficacy estimates (Logτ) of ACh in the two functional pathways with high intracellular partner coupling. *Significantly different compared with WT, $P < 0.05$, one-way ANOVA with Dunnett's post hoc test.

extend our findings to the double and triple mutants. One could suggest trying to assess the functional affinity of ACh through the use of alkylating chemical tools such as phenoxybenzamine (Khajehali et al., 2018), which would then allow us to subsequently quantify efficacy. Unfortunately, the potencies of ACh in the multiple mutants were reduced to millimolar concentrations already, and treatment with a competitive alkylating agent would push the potencies to undetectable concentration ranges.

Generally, the tyrosine lid mutations, single or multiple, did not readily affect the ground-state binding affinity of a prototypical NAM and PAM at the M_2 mAChR (Fig. 5, B and H; Fig. 6I). The major exception was the triple mutant, for which C_7/3-phth affinity was significantly increased. This is somewhat surprising, as this triple mutant is not necessarily stabilizing the inactive conformation of the M_2 mAChR as seen by a reduction in the affinity of both antagonists NMS and atropine. However, this can be explained by the fact that the absence of all three hydroxyl groups may stabilize a conformation of the M_2 mAChR for which the extracellular domain is more readily wide open and therefore more amenable to interact with NAMs (Dror et al., 2013). This suggests that the combined loss of the three hydroxyl groups stabilizes a distinct conformation of the M_2 mAChR that is biased toward NAM binding.

The cooperativity of the NAM C_7/3-phth was unaffected at all M_2 mAChR mutant constructs, with cooperativity estimates not distinguishable from high negative cooperativity ($\alpha\beta = 0$) across all functional analysis. In contrast, performing identical functional interactions between ACh and the PAM LY-2119620 at all seven M_2 mAChR mutants revealed that two residues, $Y104^{3.33}$ and $Y426^{7.39}$, were involved in the transmission of cooperativity between the orthosteric and allosteric ligands. Specifically, $Y104^{3.33}$ was critical to maintain the allosteric cooperativity in the WT receptor, whereas $Y426^{7.39}$ slightly hindered it, such that the removal of the hydroxyl group as in $Y426^{7.39}$F in single and multiple mutants allows a better transmission between the PAM and ACh. This suggests that the hydroxyl groups of $Y104^{3.33}$ and $Y426^{7.39}$ impact the transmission of cooperativity between the PAM and ACh, but do not alter the manner by which the M_2 mAChR signals to its intracellular partner (Fig. 4).

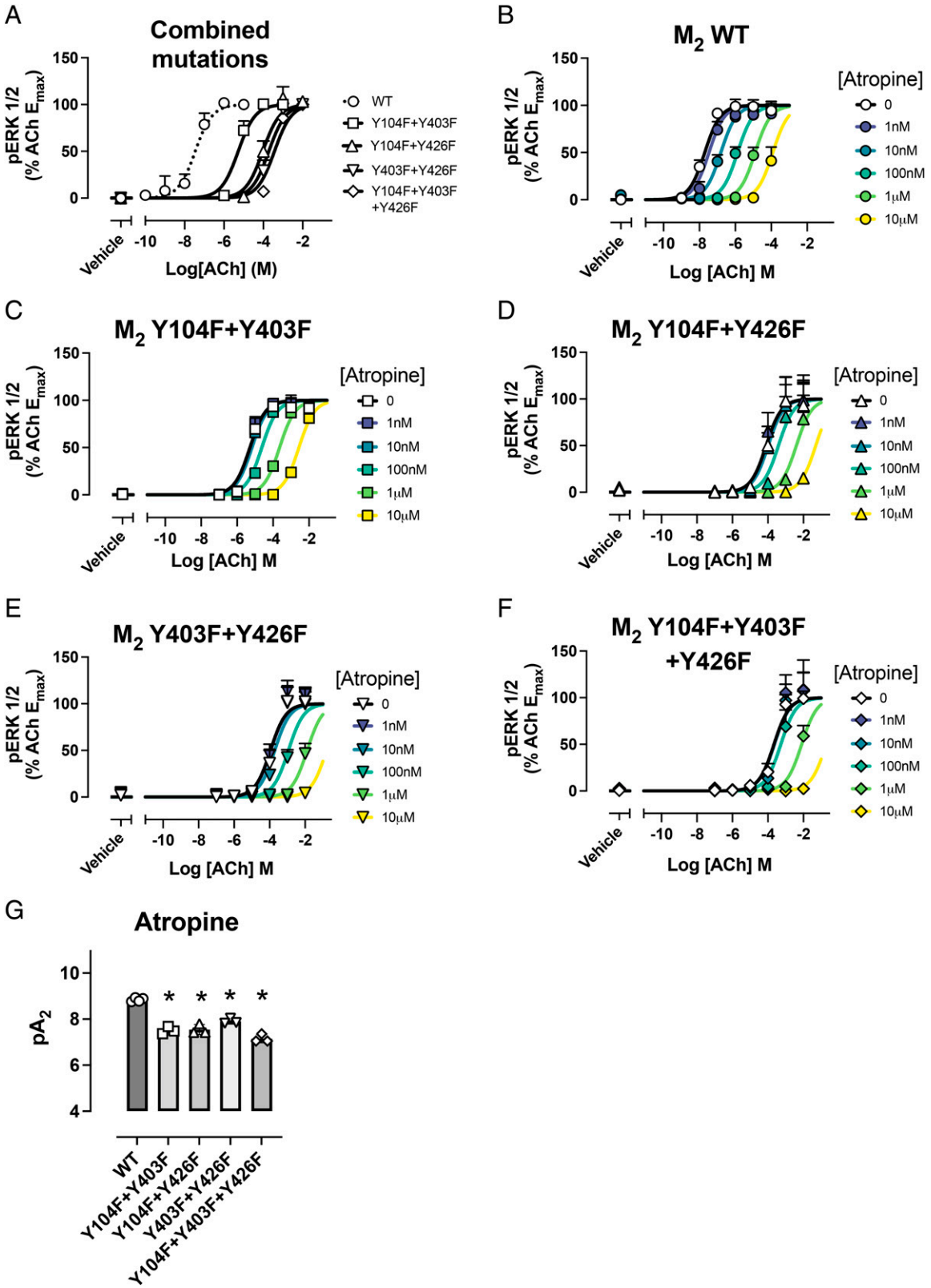

Fig. 4. Functional parameters of ACh, atropine, and NMS at the combined M_2 mAChR mutations in pERK1/2 signaling pathway. (A) Concentration-response curves of ACh at M_2 mAChR WT (dashed line), and multiple mutants (doubles and triple). Data represent mean ± S.D. of indicated number of experiments performed in duplicate and normalized to the maximal response of ACh (100%) and buffer only (0%). Grouped sizes are denoted in Supplemental Table 2. Data were fitted to the three-parameter logistic equation to quantify potency estimates. Functional interactions between ACh and atropine at the M_2 WT (B), Y104F+Y403F (C), Y104F+Y426F (D), Y403F+Y426F (E), and Y104F+Y403F+Y426F (F). Data represent mean ± S.D. of indicated number of experiments performed in duplicate and normalized to the maximal response of ACh (100%) and buffer only (0%). Grouped sizes are denoted in Table 1. Data were fitted to the Waud/Schild equation to quantify antagonist functional affinity (pA_2). pA_2 estimates for atropine (G). *Significantly different compared with WT, $P < 0.05$, one-way ANOVA with Dunnett's post hoc test.

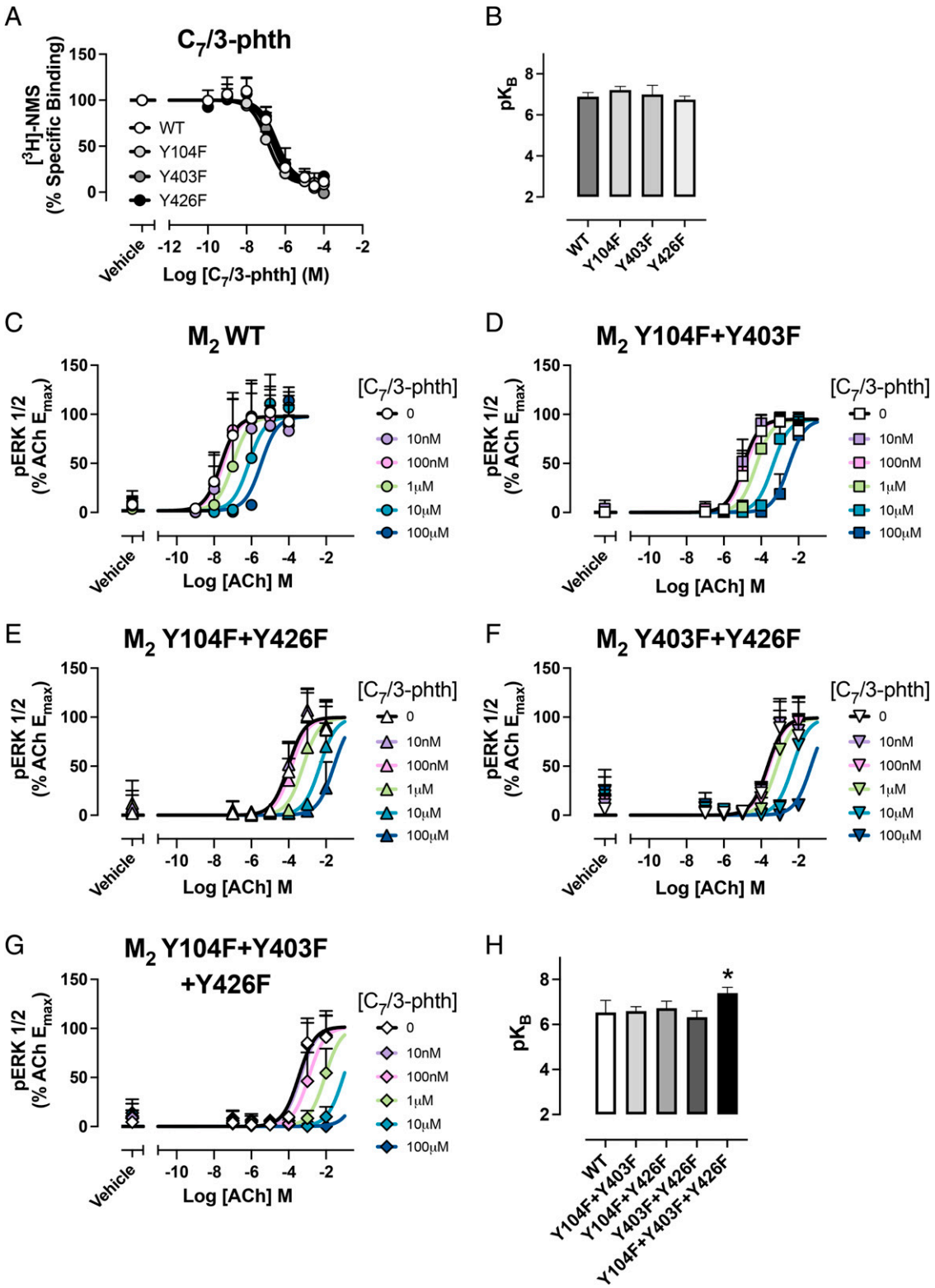

Fig. 5. Binding and functional affinity of the prototypical NAM C_7/3-phth in pERK1/2 signaling pathway at the M_2 mAChR. (A) Inhibition binding curves at the M_2 mAChR WT and all three single mutants. Data represent mean ± S.D. of indicated number of experiments performed in duplicate and normalized to vehicle only (100%) and 10 μM atropine (0%). Grouped sizes are denoted in Table 1 and were empirically fitted to a simple allosteric ternary complex model to derive estimates of allosteric modulator affinity (pK_B) and cooperativity (Logα), the latter parameter being a measure of the strength and direction of the allosteric interaction between the orthosteric and allosteric sites. (B) C_7/3-phth binding affinity (pK_B) for the allosteric site. Functional interactions between ACh and C_7/3-phth at the M_2 WT (C), Y104F+Y403F (D), Y104F+Y426F (E), Y403F+Y426F (F), and Y104F+Y403F+Y426F (G). Data represent mean ± S.D. of indicated number of experiments performed in duplicate and normalized to the maximal response of ACh (100%) and buffer only (0%). Grouped sizes are denoted in Table 1. Data were fitted to an operational model of allosterism to quantify allosteric modulator functional affinity (pK_B). (H) Functional affinity (pK_B) estimates of C_7/3-phth. *Significantly different compared with WT, $P < 0.05$, one-way ANOVA with Dunnett's post hoc test.

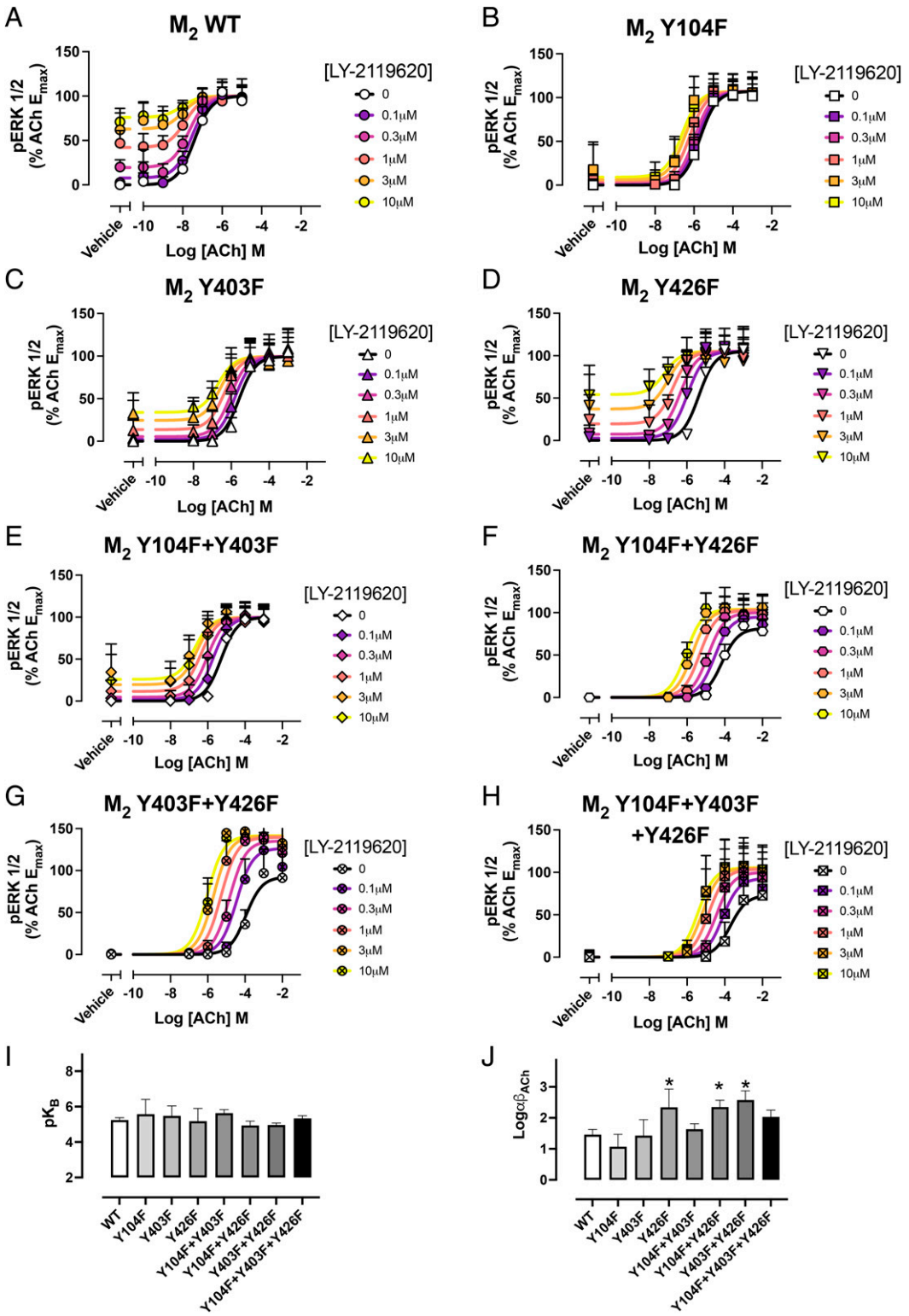

Fig. 6. Functional interactions between ACh and the PAM LY-2119620 in pERK1/2 signaling pathway at the M_2 mAChR. Functional interactions between ACh and LY-2119620 at the M_2 WT (A), Y104F (B), Y403F (C), Y426F (D), Y104F+Y403F (E), Y104F+Y426F (F), Y403F+Y426F (G), and Y104F+Y403F+Y426F (H). Data represent mean ± S.D. of indicated number of experiments performed in duplicate and normalized to the maximal response of ACh (100%) and buffer only (0%). Grouped sizes are denoted in Table 2. Data were fitted to an operational model of allosterism to quantify allosteric modulator functional affinity (pK_B), and the cooperativity between orthosteric and allosteric sites ($Log\alpha\beta$). Functional affinity (pK_B) of LY-2119620 for the allosteric site (I) and functional cooperativity ($Log\alpha\beta$) with ACh (J). *Significantly different compared with WT, $P < 0.05$, one-way ANOVA with Dunnett's post hoc test.

TABLE 2

Pharmacological parameters of functional affinity (pK_B) and functional cooperativity ($Log\alpha\beta$) of the positive allosteric modulator (PAM) LY-2119620 as determined in pERK1/2 assays, [^{35}S]GTPγS binding, and β-arrestin 2 recruitment

Values represent the mean ± S.D. of indicated number (n) of independent experiments performed in duplicate.

	pERK1/2			
Receptor	pK_B[a]	$Log(\alpha\beta)$[b]	$\alpha\beta$[c]	n
M_2 WT	5.24 ± 0.42	1.46 ± 0.51	29	9
$Y104^{3.33}F$	5.57 ± 0.83	1.01 ± 0.45	10	6
$Y403^{6.51}F$	5.48 ± 0.56	1.43 ± 0.51	27	6
$Y426^{7.39}F$	5.18 ± 0.72	2.28 ± 0.76*	191	5
Y104F+Y403F	5.63 ± 0.47	1.64 ± 0.42	44	6
Y104F+Y426F	4.94 ± 0.59	2.35 ± 0.54*	224	6
Y403F+Y426F	4.96 ± 0.27	2.58 ± 0.73*	380	6
Y104F+Y403F+Y426F	5.34 ± 0.37	2.03 ± 0.66	107	6
	[^{35}S]GTPγS			
Receptor	pK_B	$Log(\alpha\beta)$	$\alpha\beta$	n
M_2 WT	5.66 ± 0.29	1.35 ± 0.42	23	5
$Y104^{3.33}F$	5.75 ± 0.38	0.96 ± 0.23*	9	3
$Y426^{7.39}F$	5.63 ± 0.35	2.56 ± 0.38*	363	3
	β-Arrestin 2			
Receptor	pK_B	$Log(\alpha\beta)$	$\alpha\beta$	n
M_2 WT	5.89 ± 0.34	1.30 ± 0.40	20	4
$Y104^{3.33}F$	5.52 ± 0.55	0.77 ± 0.31*	6	3
$Y426^{7.39}F$	5.77 ± 0.44	2.33 ± 0.75	213	2

[a]Negative logarithm of the allosteric modulator equilibrium dissociation constant.
[b]Logarithm of the functional cooperativity between ACh and LY-2119620 in the indicated functional assay.
[c]Functional cooperativity; $\alpha\beta$ values >1 are significant of positive modulation (PAM effect).
*Significantly different compared with M_2 WT, $P < 0.05$, one-way ANOVA with Dunnett's post hoc test.

In summary, the loss of one hydroxyl group of the tyrosine lid is sufficient to reduce agonist binding affinity, whereas antagonists require the loss of multiple hydroxyl groups. In contrast to orthosteric ligands, the affinity of allosteric modulators of the M_2 mAChR, both NAM and PAM, remained unaffected, but the cooperativity between the M_2/M_4 PAM, LY-2219620, and ACh was predominantly dependent on $Y426^{7.39}$, as mutation into a phenylalanine residue increases the allosteric effect compared with the WT receptor. Perhaps surprisingly, none of the mutations appears to have any effect on the efficacy of orthosteric ligands, suggesting that the tyrosine lid is not driving the coupling of the M_2 mAChR with its intracellular partners. This is in contrast with the effect that the tyrosine residues have on the $G\alpha_{q/11}$-coupled M_3 mAChR, where mutations of the three tyrosine residues mildly affected the affinity of ACh but greatly reduced its ability to signal. A recent structure of the M_3 mAChR bound to iperoxo (Zhang et al., 2022) revealed that $Y^{7.39}$ forms a hydrogen bond with conserved residue $D^{3.32}$ due to it being in a different rotamer conformation than at the M_2 mAChR where $Y^{7.39}$ interacts with $Y^{3.33}$, providing a potential explanation for the different effects of tyrosine lid mutations between receptor subtypes (Supplemental Fig. 4C).

More broadly, our findings support the targeting of the tyrosine lid residues in the design of subtype specific orthosteric ligands, as revealed in recent structural studies of the M_1, M_2, M_3, and M_4 mAChRs (Suno et al., 2018; Brown et al., 2021; Zhang et al., 2022). For example, the M_2 mAChR-preferring antagonist AFDX 384 stabilizes a different confirmation of the tyrosine lid in comparison with the NMS-bound M_2 mAChR structure due to AFDX 384 protruding above the tyrosine lid into a subpocket between TM2/3 (Supplemental Fig. 4A). Similarly, at the M_1 mAChR, the selective agonist HTL9936 stabilizes a unique conformation of the tyrosine lid with HTL9936 protruding above the lid into a TM2/3 subpocket (Supplemental Fig. 4B). Structures of the M_3 and M_4 designer receptors exclusively activated by designer drugs (DREADDs) reveal that mutation of $Y^{3.33}$ to C abolishes ACh activity and in combination with nearby residue $A^{5.46}G$ alters the pharmacology of the receptor such that it is activated by clozapine-N-oxide (Armbruster et al., 2007; Zhang et al., 2022) (Supplemental Fig. 4D). Collectively, these studies suggest that the tyrosine lid plays in important role in the conformational dynamics of the inactive and active states of mAChRs that could be exploited for the design of subtype selective ligands.

Acknowledgments

The authors would like to thank TGR Biosciences for the generous gift of ERK1/2 phosphorylation assay reagents. This research was funded in whole or in part by the Wellcome Trust [Grant 201529/Z/16/Z]. For the purpose of open access, the author has applied a CC BY public copyright license to any Author Accepted Manuscript version arising from this submission.

Data Availability

The authors declare that all the data supporting the findings of this study are available within the paper and its Supplemental Material.

Authorship Contributions

Participated in research design: Pham, Christopoulos, Thal, Valant.

Conducted experiments: Pham, Habben Jansen, Thompson.

Contributed new reagents or analytic tools: Christopoulos, Thal, Valant.

Performed data analysis: Pham, Christopoulos, Thal, Valant.

Wrote or contributed to the writing of the manuscript: Pham, Heitman, Christopoulos, Thal, Valant.

References

Abdul-Ridha A, Lane JR, Mistry SN, López L, Sexton PM, Scammells PJ, Christopoulos A, and Canals M (2014) Mechanistic insights into allosteric structure-function relationships at the M1 muscarinic acetylcholine receptor. *J Biol Chem* **289**: 33701–33711.

Armbruster BN, Li X, Pausch MH, Herlitze S, and Roth BL (2007) Evolving the lock to fit the key to create a family of G protein-coupled receptors potently activated by an inert ligand. *Proc Natl Acad Sci USA* **104**:5163–5168.

Avlani VA, Langmead CJ, Guida E, Wood MD, Tehan BG, Herdon HJ, Watson JM, Sexton PM, and Christopoulos A (2010) Orthosteric and allosteric modes of interaction of novel selective agonists of the M1 muscarinic acetylcholine receptor. *Mol Pharmacol* **78**:94–104.

Ballesteros JA and Weinstein H (1995) Integrated methods for the construction of three-dimensional models and computational probing of structure-function relations in G protein-coupled receptors. *Methods in Neurosciences* **25**:366–428 DOI: 10.1016/S1043-9471(05)80049-7.

Black JW and Leff P (1983) Operational models of pharmacological agonism. *Proc R Soc Lond B Biol Sci* **220**:141–162.

Bourdon H, Trumpp-Kallmeyer S, Schreuder H, Hoflack J, Hibert M, and Wermuth CG (1997) Modelling of the binding site of the human m1 muscarinic receptor: experimental validation and refinement. *J Comput Aided Mol Des* **11**:317–332.

Brown AJH, Bradley SJ, Marshall FH, Brown GA, Bennett KA, Brown J, Cansfield JE, Cross DM, de Graaf C, Hudson BD, et al. (2021) From structure to clinic: design of a muscarinic M1 receptor agonist with potential to treatment of Alzheimer's disease. *Cell* **184**:5886–5901.e22.

Burger WAC, Sexton PM, Christopoulos A, and Thal DM (2018) Toward an understanding of the structural basis of allostery in muscarinic acetylcholine receptors. *J Gen Physiol* **150**:1360–1372.

Cheng Y and Prusoff WH (1973) Relationship between the inhibition constant (K1) and the concentration of inhibitor which causes 50 per cent inhibition (I50) of an enzymatic reaction. *Biochem Pharmacol* **22**:3099–3108.

Christopoulos A and Kenakin T (2002) G protein-coupled receptor allosterism and complexing. *Pharmacol Rev* **54**:323–374.

Dror RO, Green HF, Valant C, Borhani DW, Valcourt JR, Pan AC, Arlow DH, Canals M, Lane JR, Rahmani R, et al. (2013) Structural basis for modulation of a G-protein-coupled receptor by allosteric drugs. *Nature* **503**:295–299.
Eglen RM (2012) Overview of muscarinic receptor subtypes. *Handb Exp Pharmacol* (208):3–28.
Fredriksson R, Lagerström MC, Lundin LG, and Schiöth HB (2003) The G-protein-coupled receptors in the human genome form five main families. Phylogenetic analysis, paralogon groups, and fingerprints. *Mol Pharmacol* **63**:1256–1272.
Gregory KJ, Hall NE, Tobin AB, Sexton PM, and Christopoulos A (2010) Identification of orthosteric and allosteric site mutations in M2 muscarinic acetylcholine receptors that contribute to ligand-selective signaling bias. *J Biol Chem* **285**: 7459–7474.
Haga K, Kruse AC, Asada H, Yurugi-Kobayashi T, Shiroishi M, Zhang C, Weis WI, Okada T, Kobilka BK, Haga T, et al. (2012) Structure of the human M2 muscarinic acetylcholine receptor bound to an antagonist. *Nature* **482**:547–551.
Hulme EC (2013) GPCR activation: a mutagenic spotlight on crystal structures. *Trends Pharmacol Sci* **34**:67–84.
Hulme EC, Birdsall NJ, and Buckley NJ (1990) Muscarinic receptor subtypes. *Annu Rev Pharmacol Toxicol* **30**:633–673.
Keov P, López L, Devine SM, Valant C, Lane JR, Scammells PJ, Sexton PM, and Christopoulos A (2014) Molecular mechanisms of bitopic ligand engagement with the M1 muscarinic acetylcholine receptor. *J Biol Chem* **289**:23817–23837.
Khajehali E, Valant C, Jörg M, Tobin AB, Conn PJ, Lindsley CW, Sexton PM, Scammells PJ, and Christopoulos A (2018) Probing the binding site of novel selective positive allosteric modulators at the M_1 muscarinic acetylcholine receptor. *Biochem Pharmacol* **154**:243–254.
Kruse AC, Hu J, Pan AC, Arlow DH, Rosenbaum DM, Rosemond E, Green HF, Liu T, Chae PS, Dror RO, et al. (2012) Structure and dynamics of the M3 muscarinic acetylcholine receptor. *Nature* **482**:552–556.
Kruse AC, Ring AM, Manglik A, Hu J, Hu K, Eitel K, Hübner H, Pardon E, Valant C, Sexton PM, et al. (2013) Activation and allosteric modulation of a muscarinic acetylcholine receptor. *Nature* **504**:101–106.
Leach K, Sexton PM, and Christopoulos A (2007) Allosteric GPCR modulators: taking advantage of permissive receptor pharmacology. *Trends Pharmacol Sci* **28**:382–389.
Maeda S, Qu Q, Robertson MJ, Skiniotis G, and Kobilka BK (2019) Structures of the M1 and M2 muscarinic acetylcholine receptor/G-protein complexes. *Science* **364**:552–557.
Matsui H, Lazareno S, and Birdsall NJ (1995) Probing of the location of the allosteric site on m1 muscarinic receptors by site-directed mutagenesis. *Mol Pharmacol* **47**:88–98.
Nawaratne V, Leach K, Felder CC, Sexton PM, and Christopoulos A (2010) Structural determinants of allosteric agonism and modulation at the M4 muscarinic acetylcholine receptor: identification of ligand-specific and global activation mechanisms. *J Biol Chem* **285**:19012–19021.
Suno R, Lee S, Maeda S, Yasuda S, Yamashita K, Hirata K, Horita S, Tawaramoto MS, Tsujimoto H, Murata T, et al. (2018) Structural insights into the subtype-selective antagonist binding to the M_2 muscarinic receptor. *Nat Chem Biol* **14**:1150–1158.
Tautermann CS, Kiechle T, Seeliger D, Diehl S, Wex E, Banholzer R, Gantner F, Pieper MP, and Casarosa P (2013) Molecular basis for the long duration of action and kinetic selectivity of tiotropium for the muscarinic M3 receptor. *J Med Chem* **56**:8746–8756.
Thal DM, Sun B, Feng D, Nawaratne V, Leach K, Felder CC, Bures MG, Evans DA, Weis WI, Bachhawat P, et al. (2016) Crystal structures of the M1 and M4 muscarinic acetylcholine receptors. *Nature* **531**:335–340.
Valant C, Felder CC, Sexton PM, and Christopoulos A (2012) Probe dependence in the allosteric modulation of a G protein-coupled receptor: implications for detection and validation of allosteric ligand effects. *Mol Pharmacol* **81**:41–52.
Vogel WK, Sheehan DM, and Schimerlik MI (1997) Site-directed mutagenesis on the m2 muscarinic acetylcholine receptor: the significance of Tyr403 in the binding of agonists and functional coupling. *Mol Pharmacol* **52**:1087–1094.
Vuckovic Z, Gentry PR, Berizzi AE, Hirata K, Varghese S, Thompson G, van der Westhuizen ET, Burger WAC, Rahmani R, Valant C, et al. (2019) Crystal structure of the M_5 muscarinic acetylcholine receptor. *Proc Natl Acad Sci USA* **116**:26001–26007.
Waud DR and Parker RB (1971) Pharmacological estimation of drug-receptor dissociation constants. Statistical evaluation. II. Competitive antagonists. *J Pharmacol Exp Ther* **177**:13–24.
Wess J, Eglen RM, and Gautam D (2007) Muscarinic acetylcholine receptors: mutant mice provide new insights for drug development. *Nat Rev Drug Discov* **6**:721–733.
Wess J, Maggio R, Palmer JR, and Vogel Z (1992) Role of conserved threonine and tyrosine residues in acetylcholine binding and muscarinic receptor activation. A study with m3 muscarinic receptor point mutants. *J Biol Chem* **267**: 19313–19319.
Zhang S, Gumpper RH, Huang XP, Liu Y, Krumm BE, Cao C, Fay JF, and Roth BL (2022) Molecular basis for selective activation of DREADD-based chemogenetics. *Nature* **612**:354–362.

Address correspondence to: Dr. Celine Valant, Drug Discovery Biology, Monash Institute of Pharmaceutical Sciences, Monash University, 381 Royal Parade, Parkville, Victoria 3052, Australia. E-mail: celine.valant@monash.edu; or David M. Thal, Drug Discovery Biology, Monash Institute of Pharmaceutical Sciences, Monash University, 381 Royal Parade, Parkville, Victoria 3052, Australia. E-mail: david.thal@monash.edu; or Arthur Christopoulos, Drug Discovery Biology, Monash Institute of Pharmaceutical Sciences, Monash University, 381 Royal Parade, Parkville, Victoria 3052, Australia. E-mail: arthur.christopoulos@monash.edu